Anode Power in Quasisteady Magnetoplasmadynamic Accelerators

A. J. Saber* and R. G. Jahn†
Princeton University, Princeton, N.J.

Anode heat flux in a quasisteady MPD accelerator has been measured directly and locally by thermocouples attached to the inside surface of a shell anode. These measurements show that over a range of arc current from 5.5 to 44 kA, and argon mass flow from 1 to 48 g/s, the fraction of the total arc power deposited in the anode decreases from 50% at 200 kW to 10% at 20 MW. A theoretical model of the anode heat transfer asserts that energy exchange between electrons and heavy particles in the plasma near the anode occurs over distances greater than the anode sheath thickness, and hence the usual anode fall voltage, electron temperature, and work function contributions to the anode heat flux are supplemented by a contribution from the interelectrode potential. Calculations of anode heat flux using the measured current density, plasma potential, and electron temperature in the plasma adjacent to the anode agree with the direct measurements and indicate that the decrease in anode power fraction at higher arc powers can be attributed to the smaller mean free paths in the interelectrode plasma.

Introduction

THE efficiency of magnetoplasmadynamic accelerators operating below 1 MW is dominated by anode losses which may exceed 50% of the total arc power.[1-3] Consequently, considerable attention has been paid to the evaluation and understanding of anode heat transfer in such devices.[4-14] Earlier measurements in this laboratory of plasma properties adjacent to the anode indicated indirectly that the fraction of the total power delivered to the anode may decrease as arc power is increased,[15] so that a larger portion of the input power would be available for conversion to directed kinetic energy in the exhaust stream. This promise of improved conversion led to the research described herein, which involves direct measurement of anode heat flux in a quasisteady MPD accelerator over a range of arc powers from 200 kW to 20 MW, and verifies the inferred drop in fractional anode power with increasing arc power. Supplemented by measured anode plasma properties, these data are employed in an heuristic anode heat flux model based on electron transport through the discharge.

Apparatus

The quasisteady MPD accelerator[16] used in this research, its argon injection system,[17] and 160 kJ power supply[18] are shown schematically in Fig. 1. The discharge chamber is a 12.7-cm-diam × 5.1-cm-deep cylindrical cavity formed by a plexiglas cylinder 0.64-cm thick, backed by a 1-cm-thick plexiglas plate on which is centrally located a conical, 2%-thoriated tungsten cathode which is 2.7-cm long and 1.9-cm base diameter. Six nylon injectors with 4-mm diam orifices are uniformly spaced around the cathode at 2.5 cm from the chamber axis. Argon is fed to these injectors from a reservoir through a high-speed solenoid valve mounted directly behind the discharge chamber. The 3000-μF capacitor bank supplies 900-μs flat-topped, nonreversing current pulses of up to 26 kA amplitude, triggered when gas from a second reservoir and valve combination is injected into an evacuated closed chamber in series with the accelerator. The initiation of this gas-triggered switch is delayed electronically with respect to the mass pulse injected into the accelerator chamber until a steady flow of the required magnitude has been obtained—typically a few milliseconds.

The anode normally used with this accelerator is a 1-cm-thick aluminum plate with a 10.2-cm-diam orifice.[15] The present experiments, however, employed a special anode which is a 1-mm-thick shell formed to the same outer dimensions as the usual solid anode. As shown in Fig. 2, twelve #34 gage, copper-constantan thermocouples are welded directly to the inside surface of this shell anode. These thermocouples are mounted within a 15-deg azimuthal sector of the anode, and their leads pass through a hole in the anode support, which also serves as a vacuum line to the shell to preclude its distortion or rupture upon evacuation of the exhaust tank. The thermocouple cold junctions are bundled together in a glass tube sealed at one end and immersed in ice water.

The accelerator is installed in the end of a 45-cm-diam × 76-cm-long Pyrex bell jar whose background pressure of about 10^{-5} Torr is maintained by a 5.1-cm-diam oil diffusion pump. The opposite end of the bell jar is sealed with a 2.5-cm thick plexiglas slab fitted with a manual probe mount and traverse capable of moving a diagnostic probe over the anode surface and into and out of the discharge chamber without opening the tank. Terminal measurements of current and voltage are made with a Rogowski coil and a P6013 Tektronix voltage probe, respectively.

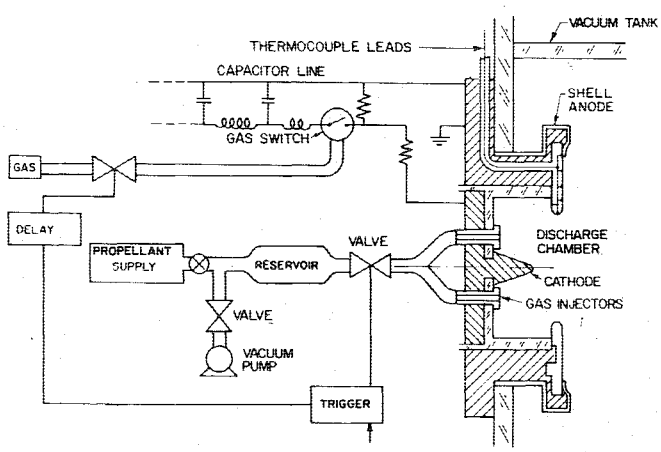

Fig. 1 MPD arcjet apparatus (schematic).

Received July 19, 1977; revision received Nov. 28, 1977.

Index categories: Electric and Advanced Space Propulsion, Plasma Dynamics and MHD.

*Presently Assistant Professor, Mechanical Engineering Dept., Concordia University, Montreal, Canada. Member AIAA.

†Dean, School of Engineering and Applied Science. Fellow AIAA.

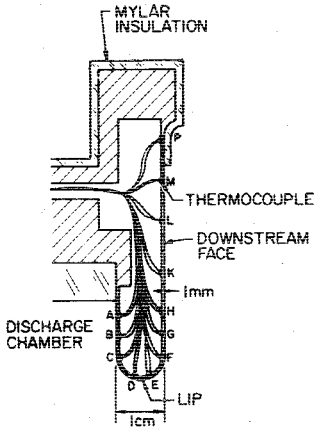

Fig. 2 Shell anode.

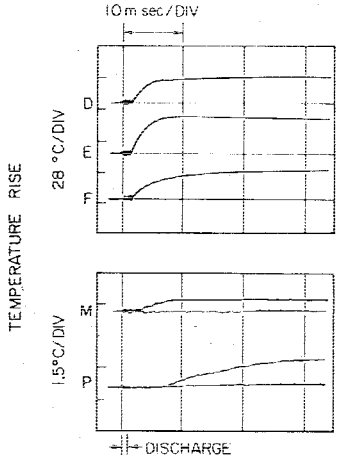

Fig. 3 Thermocouple response.

The thermocouple differential output signals are of the order of tens of microvolts and are amplified in a 12-channel, 1000× operational amplifier circuit. The hot thermocouple junction is fixed to the anode, which is the reference ground of the accelerator, and the entire amplifier system is arranged to have a small inductance and is shielded. The output is displayed on dual-beam Tektronix 555 oscilloscopes with multiple beam preamplifiers. Calibration of the anode-amplifier-oscilloscope assembly is checked by immersion of the anode in a fixed temperature water bath.

Despite all reasonable shielding efforts, it is impossible to read thermocouple signals during the discharge because of the intense electromagnetic interference. Fortunately, the thermal inertia of the anode is sufficiently high that the desired information can be obtained simply by following the temperature profiles for many milliseconds after cessation of the discharge.

Typical responses of the thermocouples to a 900-μs discharge at a current of 16 kA with an argon mass flow of 6 g/s are shown in Fig. 3. The thermocouple signals rise over several milliseconds as the heat penetrates into the shell, after which a nearly constant value is reached, modified somewhat at later times by heat conduction along the anode shell. As a control, thermocouple P lies under mylar insulation at the outer edge of the anode shell; the duration of its null response indicates the period over which conduction along the shell may be neglected and confirms the unimportance of ohmic heating in the aluminum. The data presented hereafter are extracted from the records at times after steady values have been reached, but short enough that significant heat conduction along the shell can still be neglected.

Anode Heat Flux and Power

The temperature rise of the inside surface of the anode shell is measured for discharge pulses from 5.5 to 44 kA and argon flows from 1 to 48 g/s. Typical results are shown in Fig. 4 for a 16 kA discharge with 24 g/s argon flow. The abscissa represents a linearly rolled-out anode: it traces a line of constant azimuth along the conduction surface running from the chamber insulator, around the lip (with midplane at 0.0 cm), and over the downstream face to the outer insulator. The rise in local anode temperature peaks at about 20°C just beyond the anode midplane and drops within 1 cm to less than 0.5°C on the downstream face and to about 0.1°C on the chamber side. For the measurements shown, the thermocouples were located radially in line with one of the propellant injectors; the magnitude and shape of the temperature profile are the same when the bisector between injectors is rotated to be in line with the thermocouples, indicating axial symmetry of the discharge and of the heat flux.

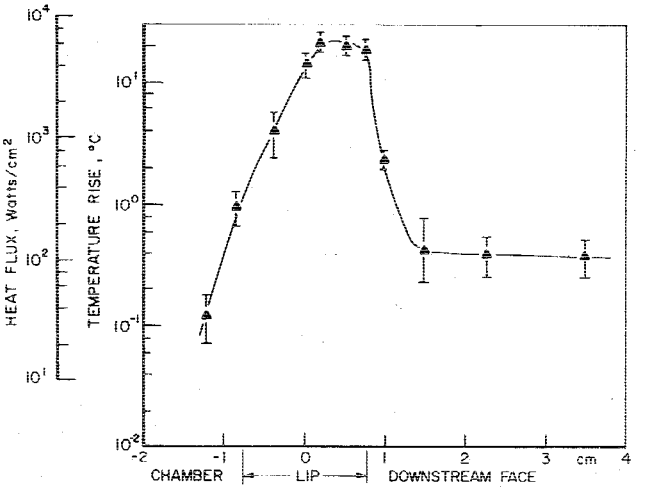

Fig. 4 Anode temperature profile (16 kA, 24 g/s).

The measured temperature rise of the thermocouples may be translated to an anode heat flux by a one-dimensional slab model.[19] The slab, of thickness l, is assumed at an initial zero temperature. A constant heat flux, F_0 W/cm^2, is then supplied to one surface for the duration of the discharge T. For times $t > T$, the temperature on the unheated side of the slab, $\theta_T(t)$, is related to F_0 by[20]

$$\theta_T(t) = F_0\left[\frac{T}{\rho l c} + \frac{l}{k}\frac{2}{\pi^2}\left\{\sum_{n=1}^{\infty}\frac{(-1)^n}{n^2} \times\left[\exp\left(-\frac{\kappa n^2 \pi^2 \tau}{l^2}\right)\right]\Bigg|_{\tau=t}^{\tau=t-T}\right\}\right] \quad (1)$$

where, for the aluminum anode,

c = specific heat = 0.216 cal/(g − °C)
ρ = density = 2.70 g/cm^3
k = thermal conductivity = 2.01 W/(cm − °C)
κ = thermal diffusivity = 0.823 cm^2/s

The series is calculated by computer and terminated when the $(n+1)$th term becomes 10^{-7} or less.

The accuracy of this relation depends on the validity of four assumptions: 1) the heat flux to the anode is constant for the duration T of the discharge with negligible initial and terminal transients, 2) heat conduction along the anode shell is negligible in comparison with the heat transfer through the shell, 3) ohmic heating in the shell can be neglected, and 4) the radius of curvature of the shell in the lip region is much larger than the shell thickness. Each of these has elsewhere been shown to be adequate within the accuracy of the data.[20]

The resulting anode heat flux for a 16 kA × 24 g/s discharge is also shown in Fig. 4. The heat flux profile resembles that of the temperature, peaking at about 6000 W/cm^2 on the lip,

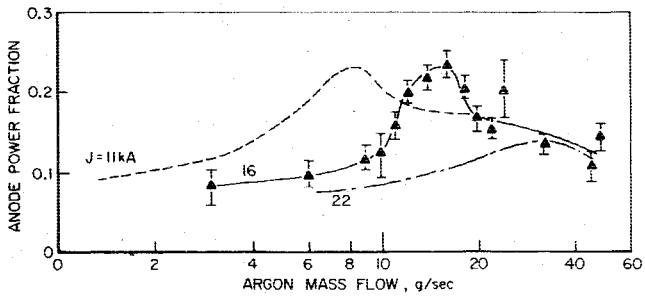

Fig. 5 Anode power fraction vs argon mass flow.

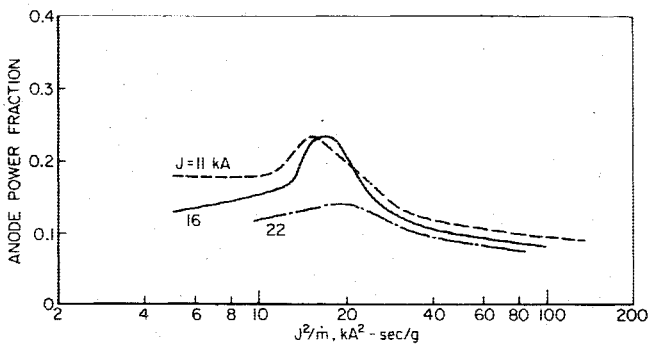

Fig. 6 Anode power fraction vs $J^2/\dot{m}$.

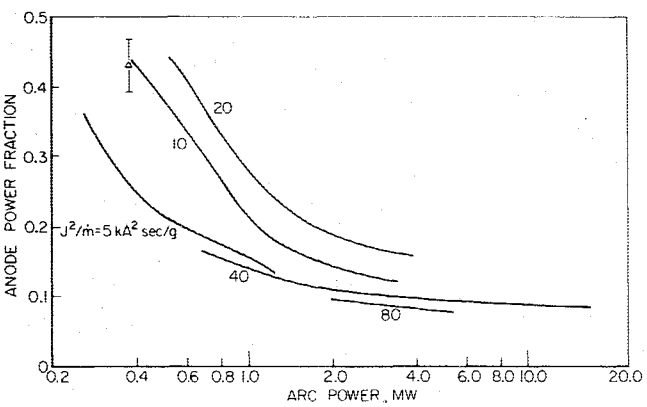

Fig. 7 Anode power fraction vs total power.

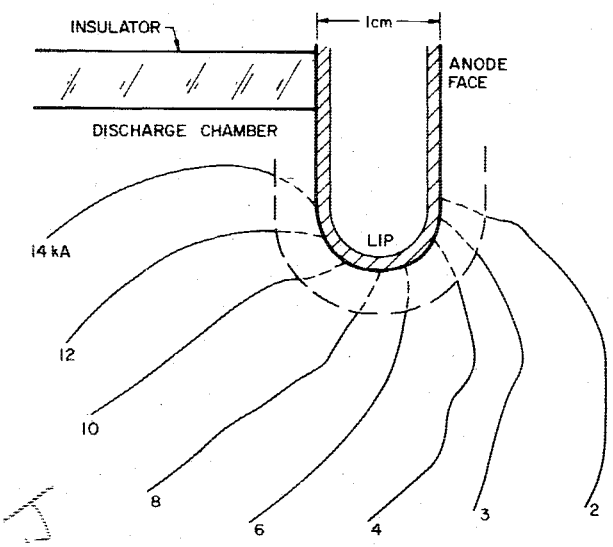

Fig. 8 Enclosed current contours (16 kA, 24 g/s).

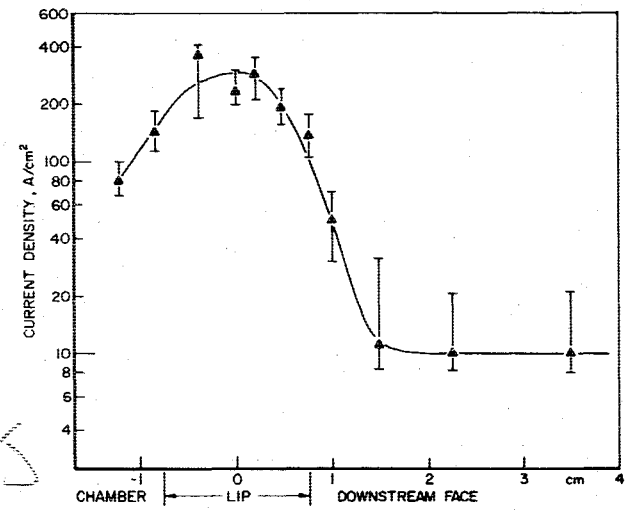

Fig. 9 Anode current density (16 kA, 24 g/s).

just downstream of the anode midplane, and dropping to 100 W/cm^2 on the face and to 40 W/cm^2 in the discharge chamber near the insulating boundary.

The anode heat flux may be integrated over the anode surface to yield the total anode power. For this purpose, the heat flux is assumed constant over the annular anode surface area between midpoints of adjacent thermocouples. The anode power derived in this way for 16 kA×24 g/s arc operation is 260 kW, some 20% of the 1.3 MW total arc power. The change of anode power fraction P_A/P_T, with injected argon flow rate, is shown in Fig. 5 for fixed arc currents of 11, 16, and 22 kA. Over the range from 1 g/s to 48 g/s, the anode power maxima shift to higher mass flow as current increases.

These maxima can be brought close to coherence through the parameter $J^2/\dot{m}$, the ratio of the square of the current to the argon mass flow, which repeatedly appears in various other contexts. For example, this ratio has served to correlate the appearance of fluctuations in arc voltage,[21] and the attainment of a maximum exhaust velocity with increasing arc current for a given mass flow.[22] When the data of Fig. 5 are replotted vs $J^2/\dot{m}$ (Fig. 6), the maxima of anode power fraction for all currents roughly coalesce at $J^2/\dot{m}$ between 15 and 20 kA^2·s/g. This value happens to coincide with the known limit of ablation-free operation of this particular arc[23]; beyond this value, the arc voltage becomes noisy and spurious operation ensues.

The general variation of anode power fraction with total arc power can now be represented using $J^2/\dot{m}$ as parameter, as shown in Fig. 7 for a range of arc power from 255 kW, the level of the highest power steady arc jets,[3,24] to 16.5 MW. Clearly, the anode power fraction decreases monotonically with increasing input power. For example, P_A/P_T drops from 45% at 400 kW to about 12% at 3.4 MW.

Note that the data in Fig. 7 cover ranges of arc operation from $J^2/\dot{m}$ = 5-10 kA^2·s/g, where ablation is not significant, to $J^2/\dot{m}$ = 20-80 kA^2·s/g, where ablation is observed.[23] The persistence of the inverse dependence of anode power fraction on arc power, even at the highest $J^2/\dot{m}$ conditions, suggests that the trend to decreasing relative anode power may also apply to vacuum or ablation arcs where the propellant is completely supplied by the ablation of a solid insulating material.[25,26]

Anode Plasma

The model commonly employed to describe anode heat flux in an arc discharge is derived from an energy balance over the anode sheath.[4,5,8] In this model, the local heat flux is related to the flow of electrons of temperature T_e at a current density j_a through an anode fall V_a to an absorbing anode of work

function ϕ:

$$q_a = j_a(V_a + (5/2)(kT_e/e) + \phi) + q_c + q_r \qquad (2)$$

where k is Boltzmann's constant, e is the electronic charge, and q_c and q_r are convective and radiative contributions which are negligible here.[20] The model in this form cannot be applied strictly to the MPD discharges under study here. In view of the much lower number densities and the non-negligible magnetic fields which prevail, the effective electron energy exchange mean free paths are not identical with the anode sheath thickness, and anode fall voltage no longer accurately represents the potential energy the electrons gain from the electric field and deliver to the anode as heat. Rather, V_a in Eq. (2) must be replaced by the voltage drop V_λ measured along the current streamline between the effective position of the last energy exchange collision and the anode surface. This energy exchange displacement λ can be expressed in terms of the magnitude of the electric field E, the mean free time between energy exchange collisions τ_e, the electron mobility μ, and the Hall parameter Ω[20]:

$$\lambda = \mu\tau_e E/\sqrt{1+\Omega^2}$$

The influence of the local magnetic field appears in the Hall parameter,[27] which acts to increase electron residence on the azimuthal magnetic field lines and therefore to decrease the net displacement.

To provide values for calculation of the modified relation (2) for comparison with the thermocouple measurements, j_a, T_e, and plasma potential V_p have been measured in the plasma adjacent to the anode with magnetic probes, and with double and floating Langmuir probes. These surveys were carried out for a fixed argon mass flow of 24 g/s with arc currents from 8 to 22 kA; for a fixed current of 16 kA with mass flows from 6 to 48 g/s; and for five combinations of current and mass flow at fixed $J^2/\dot{m} \simeq 10$ kA$^2\cdot$s/g for arc powers increasing from 0.55 to 3.4 MW.

Local anode current density is determined from enclosed current contours obtained from the integrated signals of magnetic probes, each 0.3-cm-diam, for 120 turns, in 0.4-cm-diam Pyrex tubing. Typical enclosed current contours for operation at 16 kA and 24 g/s are shown in Fig. 8, where the 1-cm-wide anode shell and discharge chamber insulating ring are indicated for reference, and the numbers on the contours indicate the total current downstream of the given line. Probing was carried to about 2 mm from the anode surface and the contours extrapolated to the anode. The corresponding anode surface current density is shown in Fig. 9. Like the heat flux profile shown in Fig. 4, the current density peaks in the lip region at about 300 A/cm^2, and falls to 80 A/cm^2 in the chamber and to 10 A/cm^2 on the downstream face. This current conduction pattern at the anode is maintained for other operating conditions of the same $J^2/\dot{m} = 10$, but as $J^2/\dot{m}$ is increased, a larger portion of the total current attaches on the downstream face of the anode.

Electron temperature is determined from the voltage-current characteristic of a double probe with 0.7-cm-long $\times$ 0.007-cm-diam electrodes.[28] Values for 24 g/s mass flow and arc currents from 8 to 22 kA are shown in Fig. 10a for a location in the anode midplane, 0.2 cm radially inward from the lip. The threefold increase, from 0.7 eV to about 2 eV, is nearly linear in arc current; in comparison, T_e is found to be less sensitive to mass flow at a given current (Fig. 10b) and to arc power at fixed $J^2/\dot{m}$ (Fig. 10c).

The local plasma potentials are derived from the measured floating potential distribution, itself obtained with a radially oriented Langmuir probe with a 0.1-cm-long $\times$ 0.007 cm-diam tungsten tip. A typical floating potential pattern is shown in Fig. 11 for 16 kA $\times$ 24 g/s operation. From the separation of the equipotentials, the electric field at the anode surface is

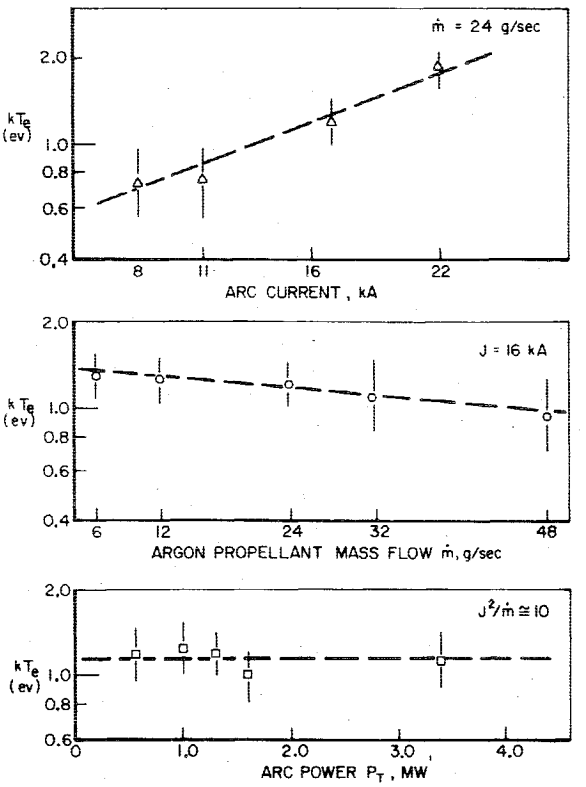

Fig. 10 Electron temperature at the anode lip.

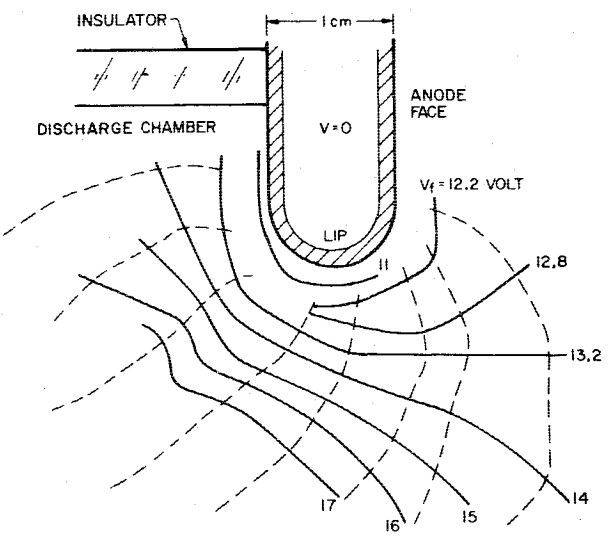

Fig. 11 Anode region floating potential (16 kA, 24 g/s).

seen to be highest on the upstream lip. Since the equipotentials are approximately normal to the current streamlines, there appears to be little tensor conduction in the anode region.

Plasma potential may be derived from floating potential by the relation[20]

$$V_f = V_p + \frac{kT_e}{e}\ln\left\{z\left(\frac{\pi m_e}{2kT_e}\right)^{1/2}\left[\left(\frac{kT_e}{m_i}\right)^{1/2} + u'\right]\right\} \qquad (3)$$

where z is the ion change number, m_e and m_i are the electron and ion masses, and u' is the ion streaming velocity component normal to the probe axis. This correction term is typically four to five times the electron temperature in electron volts.

If the anode fall voltage is taken to be the difference between the plasma potential extrapolated to the surface and the

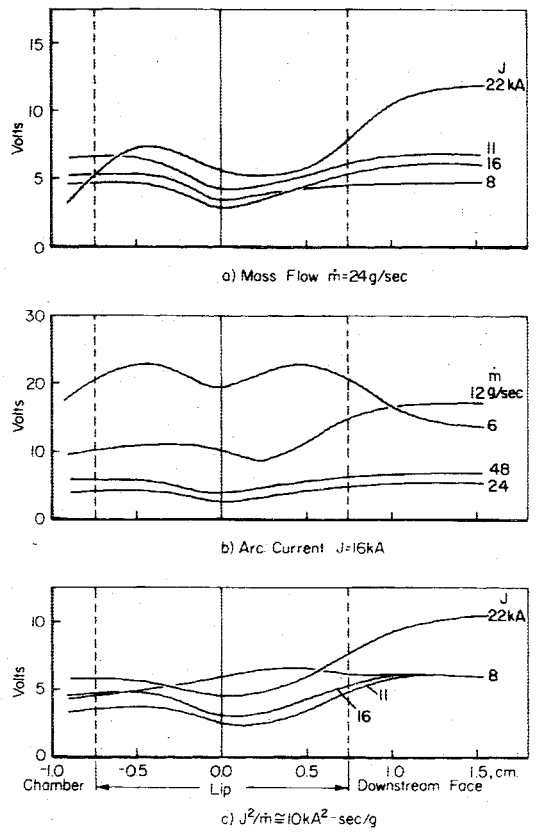

Fig. 12 Anode fall voltage.

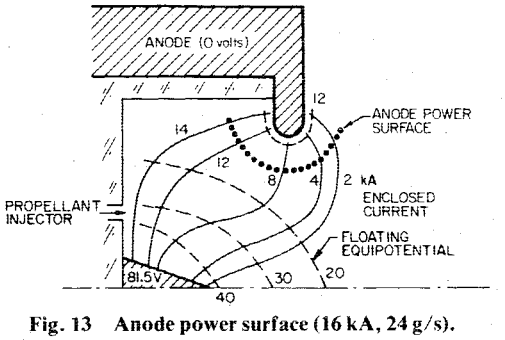

Fig. 13 Anode power surface (16 kA, 24 g/s).

anode potential, the results are shown in Fig. 12. For a current of 8 kA and a mass flow of 24 g/s (Fig. 12a), the fall voltage V_a is nearly constant at about 5 V over the anode except near the lip, where it drops to 3 V. As current is increased for the same mass flow, the voltage changes only slightly until the current reaches 22 kA, when the fall voltage over the downstream portion of the anode rises significantly. Conversely, for constant current operation at 16 kA, Fig. 12b shows little difference in anode fall as the mass flow is lowered from 48 to 24 g/s, but further reduction causes substantial increases in V_a. If the data are replotted for constant $J^2/\dot{m}$ (Fig. 12c), there is considerably less variation over the same ranges of the separate input parameters J and $\dot{m}$, again attesting the utility of this ratio. The electron density profiles needed for some portions of the calculations were determined previously from Stark-broadening of H_α and H_β impurity lines,[29] which, for the 16 kA×24 g/s discharge, yield values of about 10^{22} m^{-3} along the chamber axis, dropping an order of magnitude at the anode orifice radius.

Returning to the model underlying the modified relation (2), it remains to evaluate V_λ, the effective potential drop felt by the current-carrying electrons between their last energy exchange collision and their impact on the anode. Under the

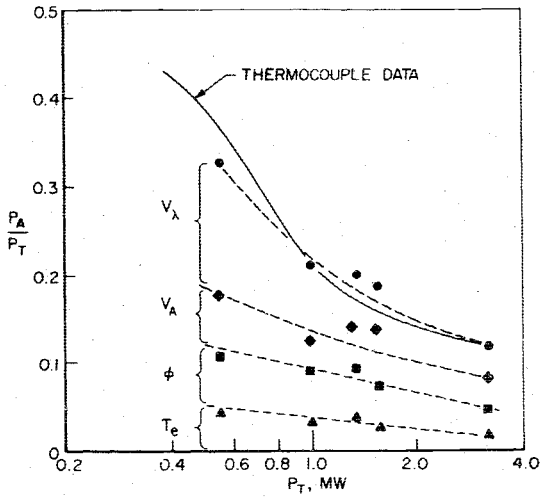

Fig. 14 Calculated anode power fraction vs total power.

prevailing conditions, the energy exchange process is dominated by elastic energy exchange collisions between electrons and ions.[20] Using the cross section for that mechanism along with electron number densities, electron temperature, and electric and magnetic fields determined from probing the plasma, the energy exchange displacement may be evaluated. The results of such a calculation are shown in Fig. 13 as an "anode power surface," i.e., the locus of points of last effective electron collision before reaching the anode. Along the 8 kA current streamline, the anode power surface lies about 1.2 cm from the anode, some one-fourth the anode orifice radius, and far outside of the usual anode fall. The plasma potential at this location is about 11 V, which is, by definition, all carried to the anode. In other words, the 4 V anode fall along the same streamline is augmented by about 7 V of interelectrode potential.

Assessing the voltage contribution to Eq. (2) in this way, the anode heat flux may then be calculated. The corresponding anode power fraction for the 16 kA×24 g/s discharge is 20% of the 1.3 MW arc power, in good agreement with the measured anode power fraction for the same operating condition. If the contribution from the interelectrode potential had been neglected, only about one-half the anode power would have been accounted for.

Figure 14 compares similar calculations[20] for other operating conditions with the measured values. In the figure, the calculated values are broken into contributions from electron temperature, work function, anode fall, and voltage from interelectrode potential, in terms of which the observed reduction of anode power fraction with increased total arc power can be rationalized. The anode work function is, of course, independent of arc power; so also, to a good approximation, is the electron temperature (Fig. 10). Hence, their contributions to the anode power fraction decrease as arc voltage rises with arc power. The anode fall, as shown in Fig. 12c, likewise increases only slightly with arc power so that its corresponding portion of the anode power fraction also decreases. Finally, the interelectrode portion of the voltage decreases with increasing arc power since the "anode power surface" moves closer to the anode because the higher plasma densities predicate shorter electron mean free paths. Indeed, at the highest powers it appears that this surface will approach anode fall dimensions, and the traditional model based on fall voltage will become a good approximation.

The same arguments also deal satisfactorily with the observed decrease of anode heat flux with increasing mass flow at fixed arc current. Anode fall voltage, electron temperature, and work function are virtually independent of mass flow; hence, their contribution to anode power fraction changes little. However, the interelectrode potential contribution to

anode power decreases with increasing mass flow, again because the associated higher densities reduce the separation of the anode power surface.

Conclusions

A series of direct thermocouple measurements of MPD anode heat flux have thus verified that anode power fraction decreases with increasing arc power, as suggested by previous indirect experiments. It follows that a larger portion of the input power is available for conversion to directed kinetic energy, and therefore that the thrust efficiency of the accelerator should be substantially higher.

Probe measurements of plasma properties in the vicinity of the anode are employed in an anode heat flux model modified for application to the MPD arc. In this model, a key ingredient is the potential difference between the anode and the location of the last effective energy exchange collision between electrons and ions before the electrons are absorbed by the anode. For the experimental conditions examined in this study, this last energy exchange collision is located well outside the anode sheath. Therefore, the energy which is added to the electron enthalpy and work function terms involves both the anode fall and an additional contribution from the potential fall outside the anode sheath. Calculation of the anode power of the MPD arc on the basis of this energy exchange model agrees well with the measurements. The decreasing fraction of input power consumed by the anode as arc power is raised results from the increased plasma density, which moves the location of the last energy exchange collision toward the anode faster than the local electric field outside the anode sheath increases.

This model may also suggest means of further reducing the anode power fraction, although many of the possibilities—such as changing arc dimensions, working fluids, or injection geometries—doubtless will cause other fundamental changes in arc behavior. One modification which has been briefly tried with some success derives from the observation that the anode fall voltage is generally lowest at the lip, where current density is a maximum. Consequently, the current conduction area of the anode was artificially restricted to a 2-mm-wide band at the anode lip. For 16 kA × 24 g/s operation, the anode power fraction in this restricted anode was approximately one-half of that for a fully exposed anode. Further exploration of this effect may be warranted.

Acknowledgments

This work was supported by NASA Grant NGL31-001-005. The authors wish to acknowledge the many helpful discussions with W. von Jaskowsky, K. Clark, and S. H. Lam, and the skillful assistance of A. Casini and D. Tregurtha in the laboratory.

References

[1] Connolly, D. J., Sovie, R. J., and Seikel, G. R., "Performance and Diagnostics of a Water-Cooled Magneto-plasmadynamic Arc Thruster," NASA TN D-5836, Lewis Research Center, Cleveland, Ohio, May 1970.

[2] Bennett, S., Enos, G., John, R. R., and Powers, W., "Magnetoplasmadynamic Thruster Research," AVSSD-0272-67-RR (NASA CR-72345), Avco Missiles, Space and Electronics Group, Space Systems Division, Lowell Industrial Park, Lowell, Massachusetts, May 1967.

[3] John, R. R., Bennett, S., and Connors, J. F., "Experimental Performance of a High Specific Impulse Arc Jet Engine," AIAA Paper 64-669, *AIAA Fourth Electric Propulsion Conference*, Philadelphia, Pa., Aug.-Sept. 1964.

[4] von Engel, A. and Steenbeck, M., *Electrische Gasentladungen*, Springer-Verlag, Berlin, 1932.

[5] Bose, T. K., "Anode Heat Transfer for a Flowing Argon Plasma at Elevated Electron Temperature," *Journal of Heat and Mass Transfer*, Vol. 15, 1972, pp. 1745-1763.

[6] Shih, K. E., et al., "Experimental Anode Heat-Transfer Studies in a Coaxial Arc Configuration," *AIAA Journal*, Vol. 6, Aug. 1968, pp. 1482-1487.

[7] Hügel, H., "Flow Rate Limitations in the Self-Field Accelerator," AIAA Paper 73-1094; also *AIAA Journal*, Vol. 12, Nov. 1974, pp. 1461-1462.

[8] Schoeck, P. A., Eckert, E. R. G., and Wutzke, S. A., "An Investigation of the Anode Losses in Argon Arcs and Their Reduction by Transpiration Cooling," University of Minneapolis, Minneapolis, Minnesota, ARL 62-341 (AD 278-570), April 1962.

[9] Eckert, E. R. G. and Pfender, E., "Advance in Plasma Heat Transfer," *Advances in Heat Transfer*, Vol. 2, edited by J. P. Harnett and T. F. Irvin, Jr., Academic Press, New York, 1967, pp. 229-316.

[10] Bez, W. and Hocker, K. H., "Theorie des Anodenfalls," *Zeitschrift für Naturforschung*, Vol. 9a, 1954, pp. 72-81.

[11] Hocker, K. H. and Bez, W., "Theorie des Anodenfalls II," *Zeitschrift für Naturforschung*, Vol. 10a, 1955, pp. 706-714.

[12] Bez, W. and Hocker, K. H., "Theorie des Anodenfalls," *Zeitschrift für Naturforschung*, Vol. 10a, 1955, pp. 714-717.

[13] Bez, W. and Hocker, K. H., "Theorie des Anodenfalls, IV. Der Anodenfall des Homogenkohle-Hochstrombogens in Luft," *Zeitschrift für Naturforschung*, Vol. 11a, 1956, pp. 118-123.

[14] Bez, W. and Hocker, K. H., "Theorie des Anodenfalls, V. Das Zischen des Homogenkohl-Hockstrombogens in Luft," *Zeitschrift für Naturforschung*, Vol. 11a, 1956, pp. 192-196.

[15] Oberth, R. C. and Jahn, R. G., "Anode Phenomena in High-Current Accelerators," *AIAA Journal*, Vol. 10, Jan. 1972, pp. 86-91.

[16] Clark, K. E., "Quasi-Steady Plasma Acceleration," Aerospace and Mechanical Sciences Report No. 859, Ph.D. Thesis, Princeton University, Princeton, N.J., May 1969.

[17] Jahn, R. G., et al., "Pulsed Electromagnetic Gas Acceleration," NASA NGL 31-001-005 *Semi-Annual Report for Period 1 July 1970 to 31 Dec. 1970*, Aerospace and Mechanical Sciences Rept. 634p, Jan. 1971, Princeton University, Princeton, N.J., pp. 64-69.

[18] Di Capua, M. S., "Energy Deposition in Parallel-Plate Plasma Accelerators," Aerospace and Mechanical Sciences Report No. 1015, Chap. 3, Ph.D. Thesis, Princeton University, Princeton, N.J., Dec. 1971.

[19] Carslaw, H. S. and Jaeger, J. C., *Conduction of Heat in Solids*, 2nd ed., Clarendon Press, Oxford, 1959, pp. 112-114.

[20] Saber, A. J., "Anode Power in a Quasi-Steady MPD Thruster," Aerospace and Mechanical Sciences Report No. 1128, Ph.D. Thesis, Princeton University, Princeton, N.J., May 1974.

[21] Malliaris, A. C., et al., "Quasi-Steady MPD Propulsion at High Power," Final Technical Report AVSD-0146-71-RR, AVCO Corporation, Feb. 1971.

[22] Jahn, R. G., et al., "Acceleration Patterns in Quasi-Steady MPD Arcs," *AIAA Journal*, Vol. 9, Jan. 1971, pp. 167-172.

[23] Boyle, M. J. and Jahn, R. G., "Effects of Insulator Ablation on the Operation of a Quasi-Steady MPD Arc," AIAA Paper 73-1090, presented at AIAA Tenth Electric Propulsion Conference, Lake Tahoe, Nev., Nov. 1973.

[24] Ducati, A. C., Giannini, G. M., and Muehlberger, E., "Recent Progress in High Specific Impulse Thermo-Ionic Acceleration," AIAA paper 65-96, presented at AIAA Second Aerospace Sciences Meeting, New York, Jan. 25-27, 1965.

[25] Vondra, R. J., Thomassen, K., and Solbes, A., "Analysis of Solid Teflon Pulsed Plasma Thruster," *Journal of Spacecraft and Rockets*, Vol. 7, Dec. 1970, pp. 1402-1406.

[26] Guman, W. J. and Williams, T. E., "Pulsed Plasma Microthruster for Synchronous Meteorological Satellite (SMS)," Paper 1066, presented at AIAA 10th Electric Propulsion Conference, Lake Tahoe, Nev., Oct. 31, 1973.

[27] Jahn, R. G., *Physics of Electric Propulsion*, McGraw-Hill, New York, 1968.

[28] Schott, L., "Electrical Probes," Chap. 11 in *Plasma Diagnostics*, W. Lochte-Holtgreven, ed., North Holland Pub. Co., Amsterdam, 1968.

[29] Jahn, R. G., et al., "Pulsed Electromagnetic Gas Acceleration," NASA NGL 31-001-005, Progress Report for Period 1 Jan. 1970 to 30 June 1970, Aerospace and Mechanical Sciences Report No. 634n, Princeton University, Princeton, N.J., July 1970, pp. 27-29.

[30] Bohm, D., "Minimum Ionic Kinetic Energy for a Stable Sheath," Chapter 3 in *The Characteristics of Electrical Discharges in Magnetic Fields*, ed. Guthrie, A. and Wakerling, R. K., McGraw-Hill, New York, 1949, pp. 77-86.